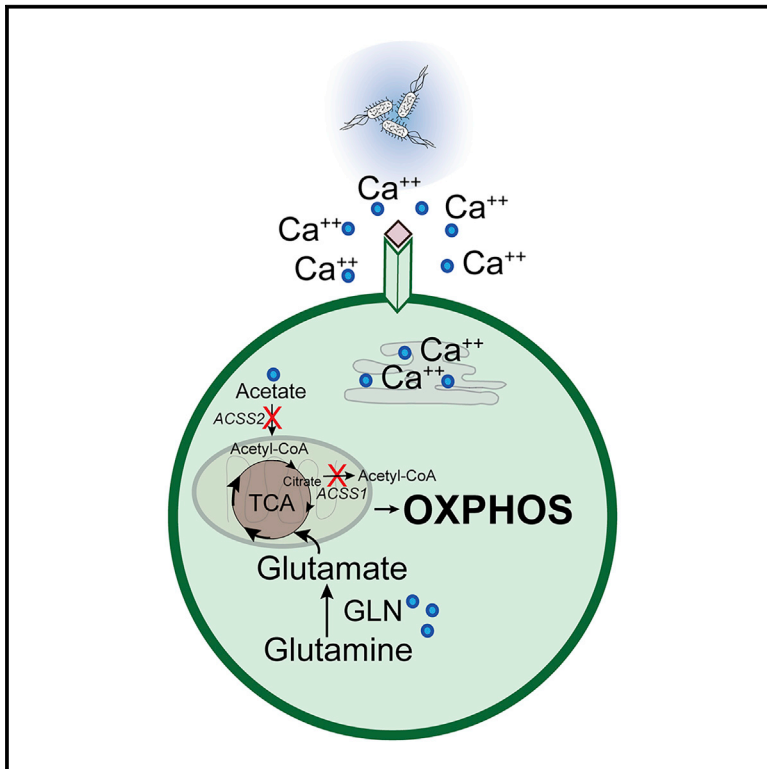


# Cell Metabolism

## Memory CD8<sup>+</sup> T Cells Balance Pro- and Anti-inflammatory Activity by Reprogramming Cellular Acetate Handling at Sites of Infection

### Graphical Abstract



### Authors

Maria L. Balmer, Eric H. Ma, Andrew Thompson, ..., Siegfried Hapfelmeier, Russell G. Jones, Christoph Hess

### Correspondence

maria.balmer@unibas.ch (M.L.B.), chess@uhbs.ch (C.H.)

### In Brief

Balmer et al. uncover that acetate abundance steadily increases at sites of inflammation. Acetate directly affects the activation and function of memory CD8<sup>+</sup> T cells by activating glutaminolysis and reducing calcium availability. *In vivo*, the integrated pro- and anti-inflammatory activities of acetate balance immune control with immunopathology.

### Highlights

- Acetate concentrations are increased at sites of inflammation
- TCR signaling and acetate reduce ACSS1/2 expression in memory CD8<sup>+</sup> T cells
- Glutaminolysis is boosted and calcium flux inhibited by acetate
- Local acetate accumulation protects from immunopathology

Short Article

# Memory CD8<sup>+</sup> T Cells Balance Pro- and Anti-inflammatory Activity by Reprogramming Cellular Acetate Handling at Sites of Infection

Maria L. Balmer,<sup>1,13,14,\*</sup> Eric H. Ma,<sup>2,3,4</sup> Andrew Thompson,<sup>5</sup> Raja Epple,<sup>1</sup> Gunhild Unterstab,<sup>1</sup> Jonas Lötscher,<sup>1</sup> Philippe Dehio,<sup>1</sup> Christian M. Schürch,<sup>6</sup> Jan D. Warncke,<sup>1</sup> Gaëlle Perrin,<sup>1</sup> Anne-Kathrin Woischnig,<sup>7</sup> Jasmin Grählert,<sup>1</sup> Jordan Löliger,<sup>1</sup> Nadine Assmann,<sup>1</sup> Glenn R. Bantug,<sup>1</sup> Olivier P. Schären,<sup>8</sup> Nina Khanna,<sup>7</sup> Adrian Egli,<sup>9,10</sup> Lukas Bubendorf,<sup>11</sup> Katharina Rentsch,<sup>12</sup> Siegfried Hapfelmeier,<sup>8</sup> Russell G. Jones,<sup>2,3,4</sup> and Christoph Hess<sup>1,5,15,\*</sup>

<sup>1</sup>Department of Biomedicine, Immunobiology, University of Basel, 4031 Basel, Switzerland

<sup>2</sup>Center for Cancer and Cell Biology, Van Andel Institute, Grand Rapids, MI, USA

<sup>3</sup>Goodman Cancer Research Centre, McGill University, Montreal, QC, Canada

<sup>4</sup>Department of Physiology, McGill University, Montreal, QC, Canada

<sup>5</sup>Department of Medicine, CITIID, Jeffrey Cheah Biomedical Centre, University of Cambridge, Cambridge CB2 0AW, UK

<sup>6</sup>Baxter Laboratory for Stem Cell Biology, Department of Microbiology and Immunology, Stanford University School of Medicine, 269 Campus Drive, Stanford, CA 94305, USA

<sup>7</sup>Department of Biomedicine, Laboratory of Infection Biology, University of Basel and University Hospital Basel, 4031 Basel, Switzerland

<sup>8</sup>Institute for Infectious Diseases, University of Bern, 3010 Bern, Switzerland

<sup>9</sup>Clinical Microbiology, University Hospital Basel, 4031 Basel, Switzerland

<sup>10</sup>Applied Microbiology Research, Department of Biomedicine, University of Basel, 4031 Basel, Switzerland

<sup>11</sup>Institute for Pathology, University Hospital Basel, University of Basel, 4031 Basel, Switzerland

<sup>12</sup>Department of Laboratory Medicine, University Hospital Basel, University of Basel, 4031 Basel, Switzerland

<sup>13</sup>Present address: Department of Diabetes, Endocrinology, Nutritional Medicine and Metabolism, Bern University Hospital, University of Bern, 3010 Bern, Switzerland

<sup>14</sup>Present address: Diabetes Center Berne, 3010 Bern, Switzerland

<sup>15</sup>Lead Contact

\*Correspondence: [maria.balmer@unibas.ch](mailto:maria.balmer@unibas.ch) (M.L.B.), [chess@uhbs.ch](mailto:chess@uhbs.ch) (C.H.)

<https://doi.org/10.1016/j.cmet.2020.07.004>

## SUMMARY

Serum acetate increases upon systemic infection. Acutely, assimilation of acetate expands the capacity of memory CD8<sup>+</sup> T cells to produce IFN- $\gamma$ . Whether acetate modulates memory CD8<sup>+</sup> T cell metabolism and function during pathogen re-encounter remains unexplored. Here we show that at sites of infection, high acetate concentrations are being reached, yet memory CD8<sup>+</sup> T cells shut down the acetate assimilating enzymes ACSS1 and ACSS2. Acetate, being thus largely excluded from incorporation into cellular metabolic pathways, now had different effects, namely (1) directly activating glutaminase, thereby augmenting glutaminolysis, cellular respiration, and survival, and (2) suppressing TCR-triggered calcium flux, and consequently cell activation and effector cell function. *In vivo*, high acetate abundance at sites of infection improved pathogen clearance while reducing immunopathology. This indicates that, during different stages of the immune response, the same metabolite—acetate—induces distinct immunometabolic programs within the same cell type.

## Context and Significance

The metabolic regulation of immunity offers opportunity for therapeutic interventions. In this approach, understanding how metabolites impact immune function at different stages of the inflammatory response is crucial. Previously, researchers at the University of Basel and their collaborators reported that with initial infection, transient acetate exposure boosts the capacity of memory T cells for glycolysis and inflammation. Here, they reveal that over time, acetate accumulates at sites of infection, where it again alters cellular metabolism and dampens T cell receptor signaling, thereby reducing the inflammatory response. Overall, they demonstrate that, depending on the stage of an immune response, one metabolite, acetate, can have distinct—and even opposing—effects on the same immune cell population.

## Q5 Q4 Q3 INTRODUCTION

Memory CD8<sup>+</sup> T cells are a small population of long-lived immune cells with protective function and unique metabolic characteristics. Effector memory (EM) CD8<sup>+</sup> T cells circulate between the blood and the periphery and migrate into various peripheral tissues, where they are exposed to constantly changing micro-environments. At tissue sites, EM CD8<sup>+</sup> T cells rapidly respond upon re-encounter of cognate antigen by producing pro-inflammatory cytokines and other effector molecules (Harty and Bado-vinac, 2008). During differentiation from naive to effector to memory cells, CD8<sup>+</sup> T cells undergo important metabolic changes, which have been intimately linked to their functional properties.

Immune cells are able to respond to their environment and acquire a variety of context-dependent fates. However, we are only beginning to understand how immune cells sense these environmental cues, and how this impacts immune cell metabolism and function. Previously we observed that systemic acetate levels rapidly increase upon infection in mice, and that, acutely, acetate at “stress levels” enhances the glycolytic capacity and effector function of EM CD8<sup>+</sup> T cells upon subsequent re-stimulation in low acetate abundance (Balmer et al., 2016). Mechanistically, in the acute scenario acetate is assimilated via acetyl-CoA synthetase 2 (ACSS2) and is expanding the cellular acetyl-CoA pool in an ATP-citrate lyase (ACLY)-dependent manner, providing acetyl groups for acetylation reactions. Acetylation of GAPDH increases its enzymatic activity, leading to increased glycolytic activity upon activation and augmented EM CD8<sup>+</sup> T cell effector function. Consistent with this finding, another report recently found an improved response to influenza infection in mice fed a high-fiber diet. In this experimental system, diet-derived short-chain fatty acids (SCFAs), including acetate, enhanced cellular metabolism of CD8<sup>+</sup> T cells, thereby boosting anti-viral activity (Trompette et al., 2018).

To redirect immune cells to sites of infection, chemokine gradients are established and modulate lymphocyte trafficking (Kunkel and Butcher, 2002). Several metabolites also guide lymphocyte migration (Sigmundsdottir and Butcher, 2008), such as sphingosine-1-phosphate (Pappu et al., 2007), retinoic acid (Iwata et al., 2004; Svensson et al., 2008), or vitamin D3 (Reiss et al., 2001).

Metabolites, including acetate, may therefore be viewed as carrying information that can alter immune cell function. Whether, in extension of this concept, metabolites impact immune cell function according to the stage of an evolving immune response has not been explored. Here we extended our study of acetate acutely and transiently accumulating in the blood circulation to its role at sites of prolonged inflammation in murine and human memory CD8<sup>+</sup> T cells.

## RESULTS

### Acetate Levels Are Increased up to 100-Fold at Sites of Infection and Suppress ACSS1 and ACSS2 Expression in CD8<sup>+</sup> T Cells

Acetate rapidly accumulates in the circulation upon systemic infection in mice (Balmer et al., 2016). Several studies have shown dramatic changes in many metabolites in the setting

of infection (Nguyen et al., 2015; Beisel, 1975; Dong et al., 2012). Here, we found that acetate accumulated in the peritoneal cavity of mice infected with *Listeria monocytogenes*, in a *Staphylococcus aureus* tissue-cage infection model, and in humans at sites of bacterial infection and inflammation (Figures 1A–1C; Table 1). We next assessed how increased local acetate levels per se impacted numbers of memory CD8<sup>+</sup> T cells in the peritoneal cavity. To this end, mice previously infected with *Listeria monocytogenes* expressing an OVA-peptide (LmOVA) were injected intraperitoneally (i.p.) with 10 mM acetate. Twenty-four hours after acetate injection, peritoneal CD8<sup>+</sup> T cell numbers in acetate-treated mice were significantly increased as compared to mice injected with PBS (Figure 1D). Most of these cells expressed phenotypic markers of memory CD8<sup>+</sup> T cells (Figure S1A). Re-challenging these mice i.p. in the presence versus absence of i.p. applied acetate also resulted in a significant acetate-dependent increase of CD8<sup>+</sup> T cells in the peritoneal fluid (Figure 1E). To assess the relation between *in vivo* accumulation of acetate at sites of inflammation and CD8<sup>+</sup> T cell counts, we analyzed leftover human fluid samples collected for clinical indications, as well as murine *Staphylococcus aureus* tissue-cage fluids. In both human and murine samples, CD8<sup>+</sup> T cell numbers and acetate abundance correlated positively up to approximately 100 mM. Beyond 100 mM acetate, CD8<sup>+</sup> T cell numbers started to decline (Figures 1F and 1G). More than 60% of the CD8<sup>+</sup> T cells recovered from tissue-cage fluid had a memory phenotype (Figure S1B). We then asked what the metabolic consequences of exposure to increased acetate abundance at sites of inflammation might be on CD8<sup>+</sup> T cells. Specifically, we tested how ACSS1 and ACSS2 were impacted in CD8<sup>+</sup> T cells 24 h after intraperitoneal injection of 100 mM acetate, as well as 24 h after intraperitoneal re-challenge of mice previously infected with LmOVA. In both models, transcript abundance of the acetate assimilating enzymes was reduced by approximately 50% (Figures 1H and 1I). Memory-like CD8<sup>+</sup> T cells can be generated *in vitro*, using an established protocol (Figure S1C) (van der Windt et al., 2012; Balmer et al., 2016). In such *in vitro* generated murine memory OT-I T cells, reduced abundance of ACSS1 and ACSS2 mRNA started to become apparent after 4 h of acetate exposure (Figures S1D and S1E). At the site of infection, cognate memory CD8<sup>+</sup> T cell activation occurs. We therefore also probed the effect of antigen-specific activation of murine memory OT-I T cells on transcript abundance of ACSS1 and ACSS2, *in vitro*. Both transcripts were strongly suppressed upon cognate re-stimulation (Figures 1J and 1K). Similar findings were made when activating human effector memory CD8<sup>+</sup> T cells in the presence of acetate (Figures S1F and S1G).

In all, these data identified high levels of acetate at sites of inflammation/infection, positively correlating with increased CD8<sup>+</sup> T cells counts up to 100 mM. We previously reported that acetate rapidly increased in the circulation of infected mice, and that, acutely, memory CD8<sup>+</sup> T cells assimilate acetate in an ACSS2-dependent manner, which leads to catalyzed glycolysis and increased IFN- $\gamma$  production (Balmer et al., 2016). We now find that exposure of CD8<sup>+</sup> T cells to increased acetate concentrations, which we show to occur at sites of infection/inflammation, evoked downregulation of ACSS1 and ACSS2, a phenomenon further accentuated by TCR activation.

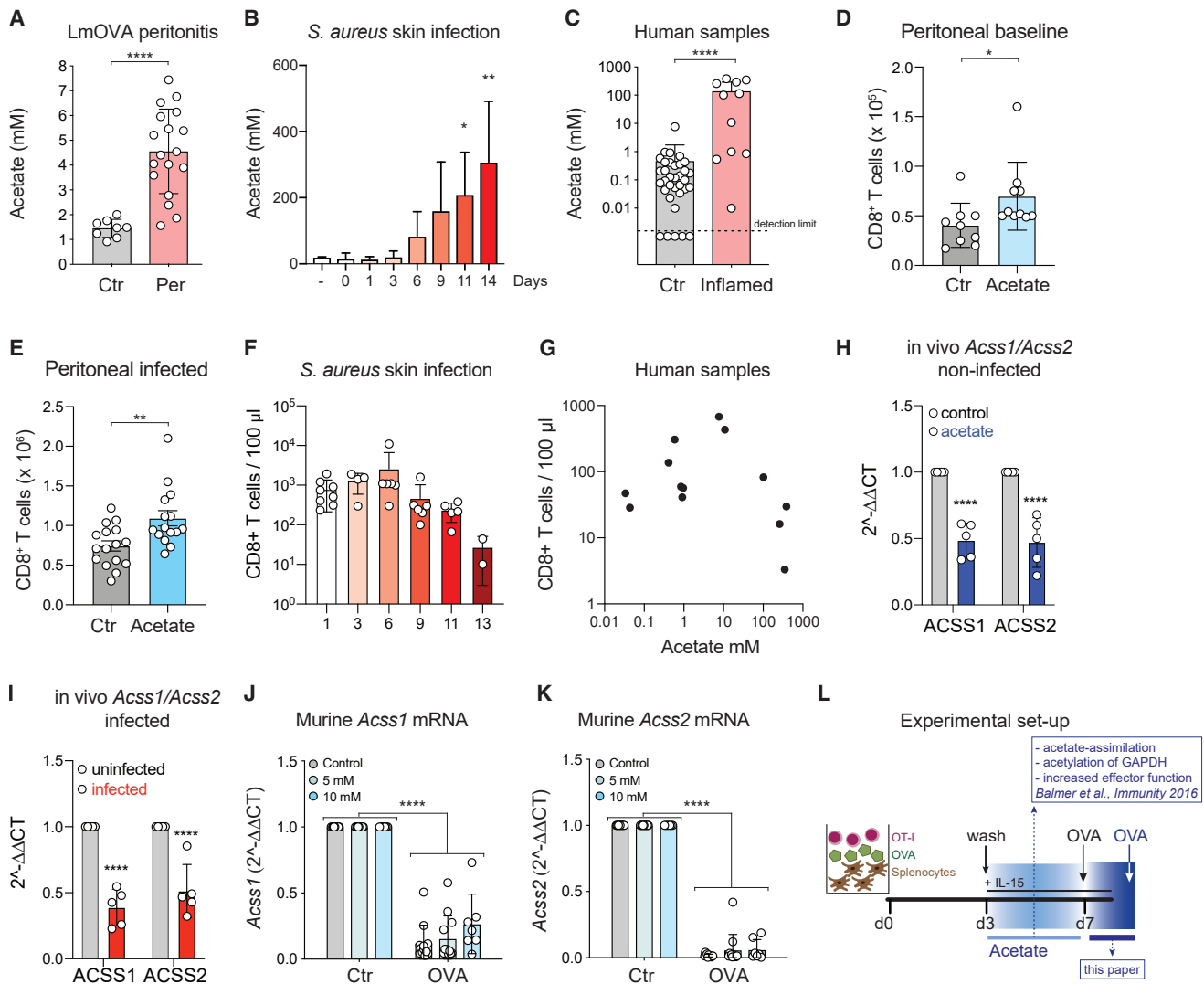


**Figure 1. Acetate Levels Are up to 100-Fold Increased at Sites of Infection and Suppress ACSS1 and ACSS2 Expression in CD8<sup>+</sup> T Cells**

(A) Acetate levels in the peritoneal fluid, 24 h after intraperitoneal LmOVA infection in C57BL/6 mice.  
 (B) Acetate levels in tissue cages at the indicated time points following *S. aureus* infection.  
 (C) Acetate levels in human-infected body fluids (abscesses) as compared to non-inflamed control fluids.  
 (D) CD8<sup>+</sup> T cell numbers in the peritoneal fluid 24 h upon intraperitoneal administration of 10 mM acetate in LmOVA-immunized mice.  
 (E) CD8<sup>+</sup> T cell numbers in the peritoneal fluid 24 h upon intraperitoneal re-infection with LmOVA  $\pm$  10 mM acetate in LmOVA-immunized mice.  
 (F and G) Absolute numbers of CD8<sup>+</sup> T cells recovered from locally infected fluids shown in (B) and (C) as determined by flow cytometry.  
 (H and I) Expression of ACSS1 and ACSS2 in MACS-purified CD8<sup>+</sup> T cells from the peritoneal cavity of LmOVA-immunized mice upon injection of 100 mM acetate (H) or re-challenged with LmOVA (I).  
 (J and K) Expression of ACSS1 (J) and ACSS2 (K) in murine memory OT-I T cells upon OVA stimulation for 4 h in the presence or absence of the indicated acetate concentrations.  
 (L) Experimental set-up mimicking the time course of acetate exposure of memory CD8<sup>+</sup> T cells.  
 Each dot represents one mouse or sample; lines indicate means. Error bars are SD. Dashed lines indicate the detection limit. t test (A and C–E), one-way ANOVA (B and F), and two-way ANOVA (H–K) were used to compare the groups. \*p < 0.05, \*\*p < 0.01, \*\*\*\*p < 0.0001.

The experimental set-up capturing these scenarios, which, *in vivo*, plausibly form a continuum, is summarized in Figure 1L.

### Acetate Promotes Glutaminolysis by Enhancing Glutaminase Enzymatic Activity

To further dissect the metabolic profile of memory CD8<sup>+</sup> T cells exposed to increased acetate levels at sites of infection, we

analyzed murine memory OT-I T cells in a metabolic flux analyzer. Supplementation of acetate resulted in a significant increase in oxygen consumption rates (OCRs) compared to medium control, whereas glycolysis was unchanged (Figures 2A and S2A). Furthermore, re-stimulation of memory OT-I T cells with OVA-peptide in the presence of acetate also increased OCR when compared to medium control (Figure S2B). Addition

**Table 1. Patient Characteristics**

Gender (f/m)	6/5
Age (mean, years)	51
Source (n)	
Abscess/cyst	7
Wound	1
Ascites	1
Synovia	2
Pathogen Isolated (n)	
<i>Staphylococcus aureus</i>	1
<i>Staphylococcus epidermidis</i>	1
Mixed	4

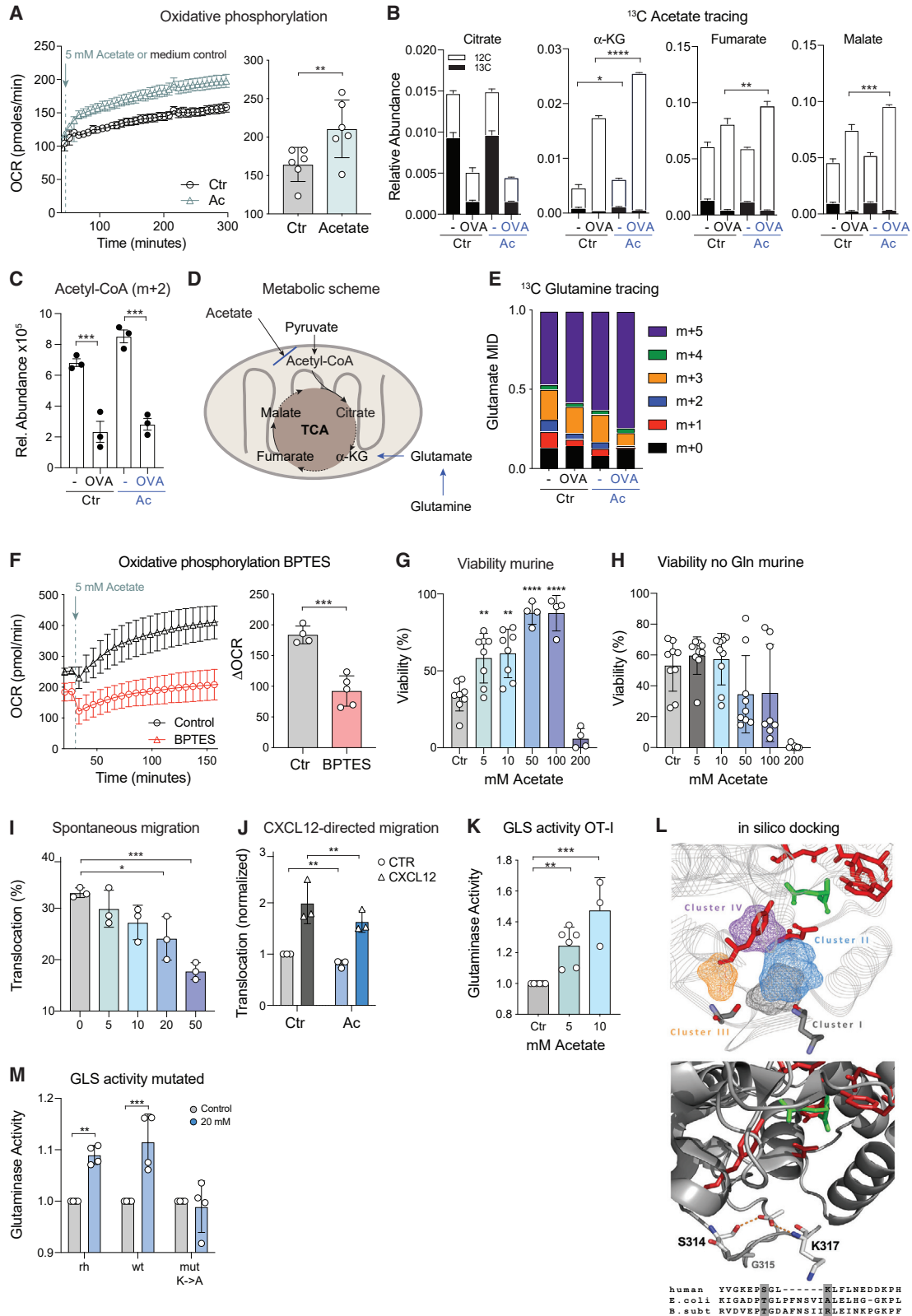
of <sup>13</sup>C-acetate to memory OT-I T cells revealed that carbon derived from labeled acetate was found in only low amounts in citrate of memory cells stimulated with OVA (Figure 2B, left panel). Albeit also only low in abundance in non-activated cells, acetate-derived carbons were consistently reduced in other intermediates of the TCA cycle (Figure 2B, right three panels). Of note, expansion of acetate-fueled acetyl-CoA was also much reduced upon OVA activation of memory CD8<sup>+</sup> T cells (Figure 2C). These data indicated that (1) acetate assimilation was blunted in these re-stimulated memory cells, and (2) increased OCR did not primarily result from increased fueling of acetate into the TCA cycle (Figure 2D). We noted, however, that the presence of acetate was associated with a higher overall abundance of  $\alpha$ -ketoglutarate, fumarate, and malate, hinting at the possibility of glutaminolysis-derived glutamate as a carbon source entering the TCA cycle (Figures 2B and 2D). To test this hypothesis, <sup>13</sup>C-glutamine tracing experiments were performed, which confirmed an increase of glutamine-derived carbons in glutamate (m+5) in the presence of acetate, both in non-activated and re-stimulated murine memory CD8<sup>+</sup> T cells (Figures 2E and S2C). This suggested that in this scenario acetate promoted increased glutaminolysis, TCA activity, and interlinked oxidative phosphorylation in memory CD8<sup>+</sup> T cells. Indeed, BPTES, an inhibitor of glutaminolysis, suppressed acetate-augmented OCR in murine and human memory CD8<sup>+</sup> T cells (Figures 2F and S2D). BPTES alone, as well as inhibition of ATP-citrate lyase, did not affect OCRs (Figures S2E and S2F). Notably, addition of acetate up to a concentration of 50–100 mM increased human and murine CD8<sup>+</sup> T cell viability (Figures 2G and S2G), a feature that was lost in the absence of glutamine in the cell culture medium (Figures 2H and S2H), or in presence of BPTES (Figure S2I). These data indicated that acetate-augmented glutaminolysis promoted increased cell respiration and viability. At sites of high acetate concentration *in vivo*, altered migratory behavior could further contribute to increased CD8<sup>+</sup> T cell numbers. We therefore also assessed spontaneous as well as CXCL12-directed migration of murine memory OT-I T cells in the presence or absence of acetate in transwell assays. In a dose-dependent manner, acetate inhibited spontaneous migration compared to medium control (Figure 2I), and also somewhat blunted chemokine-directed translocation (Figure 2J). These experiments indicated that, rather than being assimilated by members of the ACSS family and entering core metabolism, or providing acetyl

groups for acetylation reactions (Comerford et al., 2014; Balmer et al., 2016), at the site of infection acetate modulated cellular metabolism, survival, and migration in a different way.

To elucidate how acetate mediated increased glutaminolysis in memory CD8<sup>+</sup> T cells, we measured expression of glutaminase (GLS), which converts glutamine to glutamate. Addition of acetate did not change overall abundance of GLS transcript or protein (Figures S2J–S2L). By contrast, glutaminase activity was significantly increased in memory CD8<sup>+</sup> T cells exposed to acetate (Figure 2K). To dissect whether the acetate-mediated increase in glutaminase activity was a direct or indirect effect, we analyzed the activity of recombinant human glutaminase in the presence versus absence of acetate. These experiments revealed a direct and dose-dependent effect of acetate on glutaminase activity (Figure S2M), which is in line with a previous publication proposing an increase in glutaminase activity by direct binding of acetate to the enzyme (O'Donovan and Lotspeich, 1966). To rationalize this pharmacological effect, we used *in silico* ligand docking of acetate into human glutaminase co-crystallized with bound glutamine. This identified four closely located docked-pose clusters, three of which lay close to the activation loop and one close to the substrate-binding pocket (Figure 2L, upper panel). Of these, clusters I and II contained the greatest number of energetically favorable poses (7/10) and predicted interactions with residues that are known to affect the actions of other allosteric activators (Ferreira et al., 2013; Li et al., 2016). For example, the allosteric activator phosphate is similarly located in the mouse apo structure, and its actions are strongly affected by mutation of residues G320 (G315 in 3VP0) and K325 (K317 in 3PV0) in humans (Figure 2L, middle panel) (Ferreira et al., 2013; Li et al., 2016). *E. coli* and *B. subtilis* both display poor amino acid conservation in this region of the enzyme and would be predicted not to be affected by acetate (Figure 2L, lower panel). When tested we found that, indeed, acetate did not enhance *E. coli* glutaminase activity but even decreased it (Figure S2N) (Brown et al., 2008; Stalneck et al., 2017). To test, at the molecular level, the requirement of K317 for acetate to function as an allosteric activator (Figure 2L, middle and lower panel), wild-type recombinant human glutaminase (two versions: one commercially available, one mutation experiment control) and K317 → A317 mutated recombinant glutaminase were used. Again, activity of wild-type glutaminase was augmented by addition of acetate (20 mM), whereas K317 → A317 mutated glutaminase was unaffected—establishing essentiality of K317 for acetate's activity augmenting property (Figure 2M). In all, these data indicated that, upon recall, acetate promoted glutaminolysis by direct allosteric effects that increase glutaminase activity.

### Acetate Suppresses TCR Re-stimulation by Reducing Calcium Flux

We next wondered how differential acetate handling of memory CD8<sup>+</sup> T cells re-engaging with cognate antigen related to their functionality. To begin to address this question, memory OT-I T cells were re-stimulated with OVA-peptide in the presence or absence of acetate, and calcium flux was measured by flow cytometry. Acetate significantly suppressed calcium flux upon OVA re-stimulation in a dose-dependent manner (Figure 3A), suggesting decreased TCR stimulation. Accordingly, glycolytic



(legend on next page)

switching and IFN- $\gamma$  production were suppressed in the presence of acetate in a dose-dependent manner in both murine and human memory CD8<sup>+</sup> T cells (Figures 3B–3F), whereas production of TNF was unchanged (Figure S3A). Notably, calcium add-back was able to correct acetate-mediated suppression of IFN- $\gamma$  (Figure S3B). We reasoned that negatively charged acetate may interfere with biologically active (i.e., free) calcium, which would provide a mechanistic basis to the observed effect of acetate on calcium flux. We thus measured free calcium levels in the absence and in increasing concentrations of acetate, *in vitro*. To exclude protein modifications by acetate, we used PBS as a solute. In effect, free calcium levels dropped in the presence of acetate in a concentration-dependent manner (Figure 3G). Conversely, phosphate concentrations significantly increased (Figure 3H). To assess whether acetate also depleted calcium levels *in vivo*, we determined free calcium levels in murine and human fluids sampled from infectious and inflamed sites. Calcium levels were significantly depleted in both human-infected and sterile inflamed body fluids, and infected murine peritoneal fluids in the presence of acetate (Figures 3I and 3J). Inversely, phosphate levels were increased in murine *S. aureus* skin infection and in inflamed human body fluids (Figures 3K and 3L). To elucidate whether decreased calcium levels were responsible for reduced calcium flux upon TCR re-stimulation, we added excess calcium to acetate-exposed memory OT-I T cells upon OVA re-stimulation. Addition of 10 mM calcium was sufficient to normalize calcium flux back to control conditions (Figures 3M and S3C). Addition of 10 mM calcium was also sufficient to augment memory OT-I T cell migration, indicating that impaired cell activation and migration in the presence of acetate may be related to calcium depletion in the presence of acetate (Figure S3D). Of note, in the absence of glutamine, acetate also reduced IFN- $\gamma$  production by memory OT-I T cells, indicating that the effect of acetate on glutaminase

activity and its effect on calcium flux are distinct (data not shown). These data established that acetate suppressed memory CD8<sup>+</sup> T cell re-call responses as a consequence of reduced calcium availability when present during re-stimulation. To directly capture acetate's time- and concentration-dependent immune augmenting versus immuno-suppressive features, a time course experiment encompassing both features of this metabolite was performed (Figure 3N).

### Acetate Suppresses Immunopathology at Sites of Infection and Modulates Tissue Remodeling

We went on and asked how, at the site of infection, acetate-mediated metabolic and functional re-programming of memory CD8<sup>+</sup> T cells modulated immune control. To address this question, we re-infected mice previously infected with LmOVA *i.p.* in the presence or absence of 10 mM acetate also administered *i.p.* at the same time as the pathogen. Similar to our previous findings, acetate promoted superior immune control as measured by bacterial loads in the liver and spleen (Figure 4A). However, immunopathology determined by local lactate dehydrogenase levels, as well as peritoneal IFN- $\gamma$ , was suppressed in the presence of acetate (Figures 4B and 4C). Peritoneal concentrations of IL-10 tended to be elevated in the presence of acetate, indicating a possible immunomodulatory role of acetate (Figure S4A). Increased expression of PD-L1 on CD8<sup>+</sup> T cells recovered from peritoneal fluid would also align with this notion (Figure S1A). Histologically, peritoneal thickness—as another measure of immunopathology (Mizuno et al., 2009)—was also reduced in the presence of acetate (Figure 4D). To further characterize a potential immunomodulatory role of acetate at the site of infection, we performed a PCR array from peritoneal tissue of mice re-challenged with LmOVA in the presence or absence of acetate. This experiment revealed increased TGF- $\beta$  transcript levels in the peritoneum from acetate-treated mice, whereas

### Figure 2. Acetate Promotes Glutaminolysis by Enhancing Glutaminase Enzymatic Activity

(A) Memory OT-I T cells were analyzed by metabolic flux analysis upon injection of 5 mM acetate (blue) or medium control (black) at the beginning of the analysis (dashed line and arrow). Shown is a representative experiment of OCR values and pooled data from 5 independent experiments showing OCR values at 300 min post-injection.

(B and C) <sup>13</sup>C-acetate tracing experiment of murine memory OT-I T cells. Cells were incubated  $\pm$  5 mM <sup>13</sup>C-acetate (blue) and  $\pm$  10  $\mu$ M OVA-peptide for 6 h and then all traced with <sup>13</sup>C-acetate for 6 h.

(B) Filled bars represent contribution of <sup>13</sup>C-acetate to the respective metabolite pool.

(C) Relative abundance of m+2 acetyl-CoA from <sup>13</sup>C-acetate.

(D) Schematic of mitochondrial metabolism and possible effects of acetate.

(E) Same experiment as in (B), but with <sup>13</sup>C-glutamine. The different colors indicate the number of radiolabeled carbons detected in glutamate.

(F) Memory OT-I T cells were pre-incubated for 2 h in the presence (red) or absence (black) of the glutaminolysis inhibitor BPTES or vehicle control. Cells were then analyzed by metabolic flux analysis upon injection of 5 mM acetate (dashed line and arrow). Shown is a representative experiment of OCR values and pooled data from 4 independent experiments assessing the net increase in OCR between 30 and 150 min.

(G and H) Viability of murine memory CD8<sup>+</sup> T cells cultured *in vitro* for 3 days in the presence (G) or absence (H) of glutamine and increasing acetate concentrations as determined by flow cytometry (% Annexin V and PI negative).

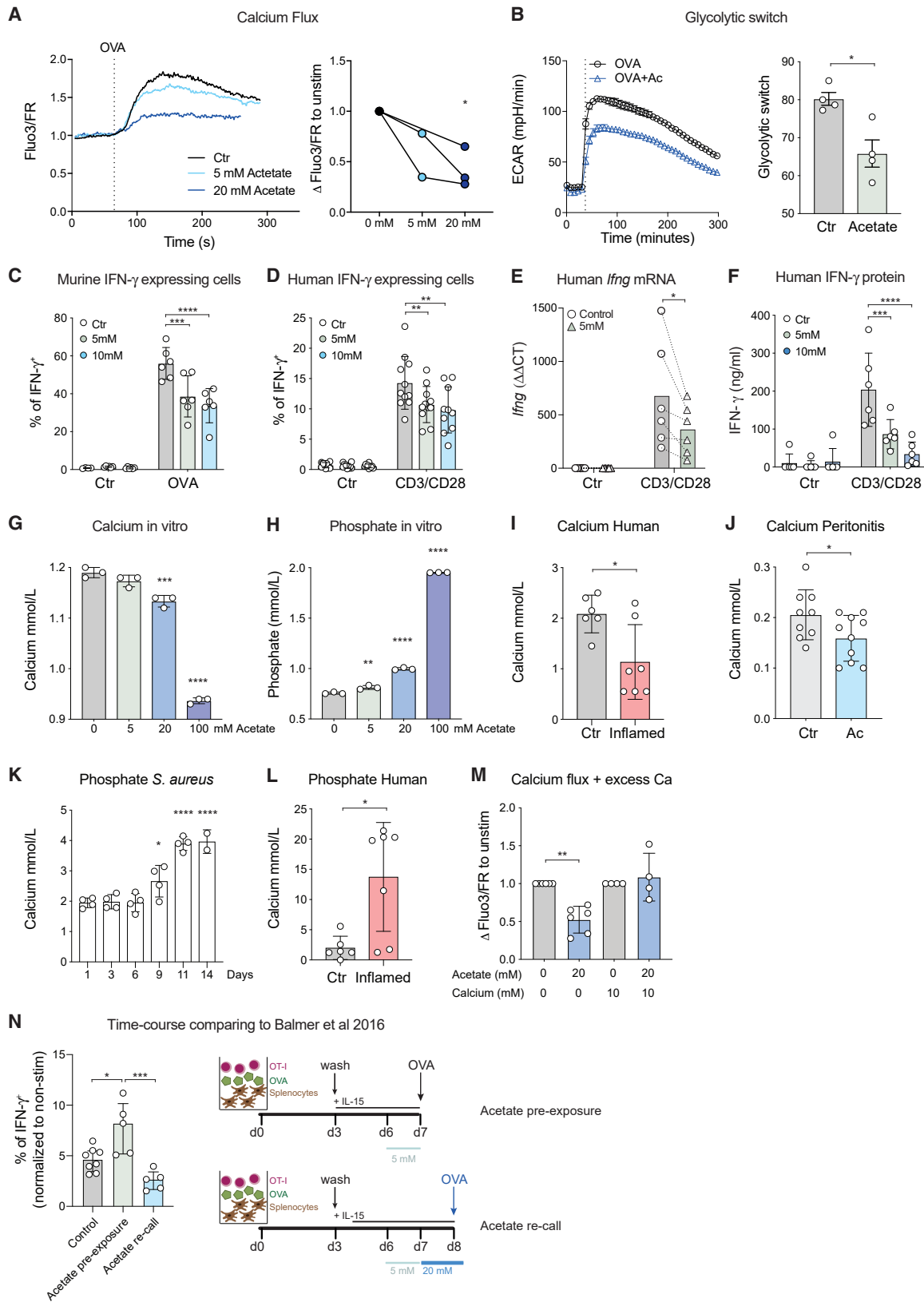
(I and J) Spontaneous (I) and chemokine-directed (J) migratory capacity of *in vitro* generated murine memory OT-I T cells analyzed in a transwell assay in increasing concentrations of acetate.

(K) Glutaminase activity in murine memory OT-I T cell extracts exposed for 4 h to the indicated acetate concentrations.

(L) Upper panel: a wireframe representation of the four docked pose clusters identified in our study is shown in one of the four subunits of the enzymatically active homo-tetramer of glutaminase. Middle: an example docked pose from cluster I, showing predicted hydrogen bond interactions (dashed orange lines) between acetate and the side chains of residues S319 (314) and K235 (317). The green molecule is bound glutamine. Bottom: an alignment showing the poor amino acid conservation in the predicted allosteric activation region of human (from the 3PVO crystal structure used here) and prokaryotic glutaminase (P77454, *E. coli*; O31465, *B. subtilis*). The gray shade highlights S314 and K317.

(M) Glutaminase activity of human recombinant glutaminase (rh), wild-type human glutaminase (wt, mutation control), and human glutaminase with a K  $\rightarrow$  A mutation at position 317, depicted in the lower panel of (L), assessed in the presence or absence of 20 mM acetate.

Each dot represents one mouse or human; lines indicate means. Error bars are SD. t test (A and F), one-way ANOVA (G–I and K), or two-way ANOVA (B, C, J, and M) was used to compare the groups. \*p < 0.05, \*\*p < 0.01, \*\*\*p < 0.001, \*\*\*\*p < 0.0001.



(legend on next page)

transcripts of the pro-inflammatory cytokines *Irfng* and *Tnf*, as well as transcripts of integrin- and collagen-family genes, were decreased in the presence of acetate (Figures 4E and S4B). Overall, these experiments suggested that, at the site of infection, acetate suppressed immunopathology.

Taken together, our data indicated that at sites of infection, acetate catalyzed glutaminolysis in memory CD8<sup>+</sup> T cells, augmenting mitochondrial respiration and cell survival. Further, by altering availability of free calcium, acetate suppressed TCR-triggered calcium flux, glycolytic switching, and IFN- $\gamma$  production. In a time-resolved manner, acetate's glycolysis boosting capacity (Balmer et al., 2016) and the herein described effects were balancing pathogen clearance against immunopathology (Figure 4F).

## DISCUSSION

The metabolic environment has been shown to critically impact the outcome of immune responses. Probably the best characterized example is the tumor microenvironment, which shapes immune cell metabolism and function. Here we show that acetate levels accumulate at sites of infection and reprogram memory CD8<sup>+</sup> T cell metabolism and function by boosting glutaminolysis and altering availability of calcium. Acetate levels can rise up to about 5 mM in the circulation upon systemic bacterial infection in mice (Balmer et al., 2016). At the site of infection, acetate levels are initially low but then can reach >100 mM. This implies that memory T cells are exposed to rising acetate concentrations at inflamed sites where they are likely to re-encounter antigen. While acute, transient exposure of ACSS competent memory CD8<sup>+</sup> T cells to acetate levels of 5 mM boosted glycolysis and cytokine secretion (Balmer et al., 2016), acetate also mediated a decrease of its assimilation machinery (i.e., ACSS1 and 2). On the one hand, non-metabolized acetate augmented glutaminase enzymatic activity, fueling the TCA cycle and mitochondrial respiration, thereby supporting cell viability. On the other hand, acetate present during antigen re-encounter reduced free calcium abundance, thus suppressing migration and TCR-triggered calcium flux, and subsequent effector function. This indicates that, before reaching the site of infection, memory CD8<sup>+</sup> T cells are boosted and thus prepared for rapid pathogen removal at acutely infected sites (Balmer

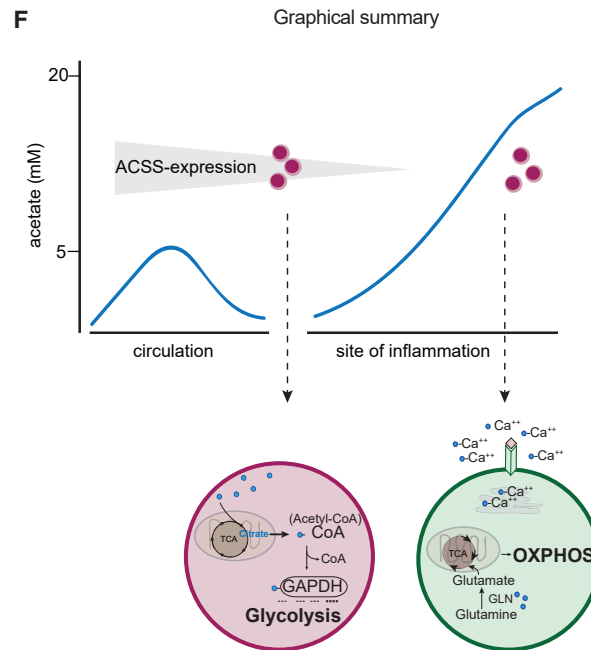
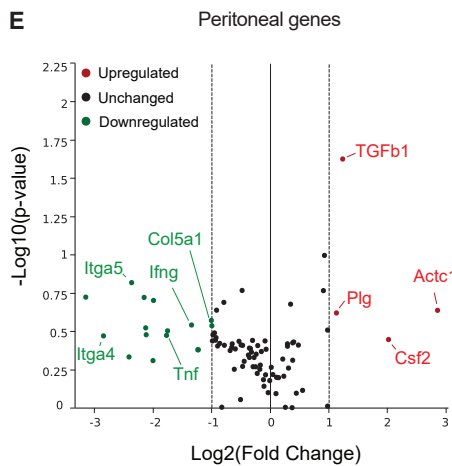
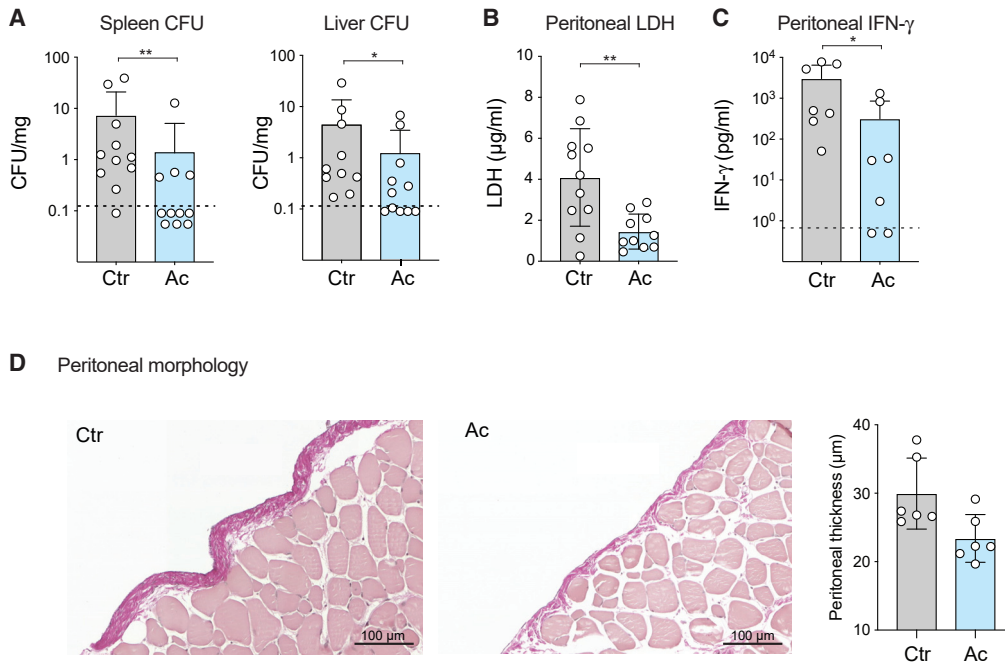
et al., 2016). However, at the site of unresolved inflammation where acetate abundance is steadily increasing, their inflammatory capacity is gradually being suppressed, thereby balancing pathogen clearance and immunopathology. Depending on timing of exposure, the same metabolite—acetate—thus has opposing effects on memory CD8<sup>+</sup> T cells: in transit to the site of infection acetate is used to acetylate and catalyze GAPDH, enhancing glycolytic switch and interlinked inflammatory output of memory CD8<sup>+</sup> T cells early upon re-stimulation (i.e., when re-stimulated in low acetate abundance). At sites of prolonged inflammation, where acetate gradually accumulates, cells lose their capacity to assimilate acetate, and acetate catalyzes glutaminase activity and develops suppressive capacity by “buffering” calcium (Figure 4F). Mechanistically, acetate's effects on glutaminase activity and calcium flux are distinct. However, functionally they may well complement each other. Initially, prolonged survival allows for sufficient cell numbers available for efficient pathogen clearance, while later on this may support accumulation of inflammation resolving mediators.

Immunopathology plays a key role in many infectious and inflammatory diseases, contributing to morbidity and mortality. For example, during viral infections cytotoxic CD8<sup>+</sup> T cells, while effectively killing infected cells, can also cause non-specific, tissue-destructive inflammation (Rouse and Sehrawat, 2010). Likewise, immunopathology mediates autoimmune and chronic inflammatory diseases, such as inflammatory bowel disease. In the intestine, acetate concentrations reach up to 200 mM/kg wet weight (Huda-Faujan et al., 2010; Høverstad and Midtvedt, 1986), and were significantly reduced in patients with inflammatory bowel disease, indicating that these high acetate concentrations contribute to host-microbial mutualism and may protect from immunopathology (Huda-Faujan et al., 2010).

Acetate is an SCFA abundantly produced by the gut microbiota via fermentation of dietary fibers (Tremaroli and Bäckhed, 2012). However, germ-free animals also readily increase serum acetate levels upon metabolic stress, indicating efficient release of acetate from endogenous sources (Balmer et al., 2016). Further, we previously demonstrated that rising systemic acetate levels upon systemic bacterial infection are also not primarily bacteria-driven, since systemic infection with bacteria genetically incapable for acetate production induced stress levels of acetate in the host (Balmer et al., 2016). The source, or sources,

### Figure 3. Acetate Suppresses TCR Re-stimulation by Reducing Calcium Availability

(A) Calcium flux as assessed by flow cytometry of murine memory OT-I T cells cultured in the presence (blue) or absence (black) of acetate for 30 min. One representative experiment (left) and pooled data from 2–3 independent experiments (right) are shown.  
(B) Glycolytic switch upon OVA injection with (blue) or without (black) acetate in murine memory OT-I T cells as assessed by metabolic flux analysis. One representative experiment (left) and pooled data from 4 independent experiments (right) are shown. The glycolytic switch was calculated by subtracting the basal ECAR from maximal ECAR. The dashed line indicates the time of OVA ( $\pm$  acetate) injection.  
(C and D) IFN- $\gamma$  production as assessed by intracellular cytokine staining in murine (C) or human (D) memory CD8<sup>+</sup> T cells 4 h after re-stimulation with 10  $\mu$ M OVA-peptide or anti-CD3/CD28 antibodies in the presence (blue) or absence (black) of indicated acetate concentrations.  
(E and F) IFN- $\gamma$  mRNA (E) and protein (F) in human memory CD8<sup>+</sup> T cells 4 h after re-stimulation with anti-CD3/CD28 antibodies in the presence (blue) or absence (black) of indicated acetate concentrations.  
(G and H) Calcium (G) and phosphate levels (H) assessed *in vitro* in the presence (blue) or absence (black) of the indicated acetate concentrations.  
(I–L) Calcium (I and J) and phosphate levels (K and L) in human and murine fluids as described in Figures 1A–1C.  
(M) Calcium flux as described in (A) was assessed in the presence (blue) or absence (black) of acetate and additional calcium.  
(N) IFN- $\gamma$  production as assessed by intracellular cytokine staining in murine memory OT-I T cells exposed to acetate either prior to or during OVA re-stimulation for 4 h.  
Each dot represents one mouse or human; lines indicate means. Error bars are SD. t test (B, I, J, and L), one-way ANOVA (G, H, K, M, and N), or two-way ANOVA (C–F) was used to compare the groups. \*p < 0.05, \*\*p < 0.01, \*\*\*p < 0.001, \*\*\*\*p < 0.0001.



Exposure of CD8<sup>+</sup> T to circulation stress-levels of acetate, re-stimulation in absence of acetate → mimicking entrance of these cells into acute inflammatory site with (at this early stage) low acetate abundance:

→ Acetate is assimilated and expands acetyl-CoA  
→ acetylation of GAPDH  
→ catalyzing glycolysis and interlinked IFN $\gamma$  production

**PRO-INFLAMMATORY**

(Balmer, Immunity 2016)

Re-stimulation of memory CD8<sup>+</sup> T cells in presence of acetate → mimicking later-stage inflammatory site:

→ Acetate and TCR-signal driving shut down of ACSS: acetate assimilation blocked  
→ acetate dampening TCR driven calcium-flux  
→ acetate directly binding and activating glutaminase

**ANTI-INFLAMMATORY**

(Balmer - current submission)

(legend on next page)

of increased local acetate levels observed in this study thus remain unclear. Since at sterile inflammatory sites acetate abundance was also increased, a bacterial origin seems unlikely. Given the large amount of cell death within any inflammatory area, one possibility could be the accumulation of extracellular acetate that is released from intracellular sources upon cell death.

In conclusion, our data demonstrate that acetate can function as a rheostat of the immune response, balancing pro- and anti-inflammatory properties during the course of an immune response. Opposing effects on immune cell function driven by a single metabolite through distinct cellular metabolic effects emphasize the need to consider metabolic reprogramming in a time- and context-resolved manner.

### Limitations of Study

The molecular mechanisms by which acetate and TCR signaling drive downregulation of ACSS1 and ACSS2 remain to be defined. Also, we could not measure memory CD8<sup>+</sup> T cell metabolism in real time *in vivo* during the course of an infection but focused on *ex vivo* analyses. Finally, while we also found increased accumulation of acetate at sites of inflammation in humans, how memory CD8<sup>+</sup> T cell metabolism is regulated at these sites needs to be explored.

### STAR★METHODS

Detailed methods are provided in the online version of this paper and include the following:

- KEY RESOURCES TABLE
- RESOURCE AVAILABILITY
  - Lead Contact
  - Materials Availability
  - Data and Code Availability
- EXPERIMENTAL MODEL AND SUBJECT DETAILS
  - Animal Husbandry
  - Human Abscess Fluids
  - Isolation of Human Effector Memory (EM) CD8<sup>+</sup> T Cells
  - Cell Culture
- METHOD DETAILS
  - *In Vitro* Memory Differentiation
  - Acetate Measurement in Murine and Human Samples
  - Measurement of Cell Viability
  - Transwell migration assay
  - Murine Peritonitis Model
  - *S. aureus* Tissue Cage Model

- Histology
- Seahorse Experiments
- Metabolic Tracing
- Quantitative PCR
- Glutaminase Activity Assay
- Glutaminase-Acetate *In Silico* Docking
- Glutaminase Mutagenesis
- Calcium Flux
- Calcium and Phosphate Quantification
- Intracellular Cytokine Staining
- Cytometric Bead Array
- Immunoblot Analysis
- QUANTIFICATION AND STATISTICAL ANALYSIS

### SUPPLEMENTAL INFORMATION

Supplemental Information can be found online at <https://doi.org/10.1016/j.cmet.2020.07.004>.

### ACKNOWLEDGMENTS

M.L.B. was supported by SNSF grant PMPDP3\_171261/1 and Novartis Foundation grant 17C141. C.H. was supported by SNSF grants 31003A\_172848 and 310030\_192677. **Q8**

### AUTHOR CONTRIBUTIONS

M.L.B. designed, performed, and analyzed most experiments and wrote the manuscript; E.H.M. and R.G.J. performed metabolic tracing experiments; A.T. performed *in silico* docking experiments; R.E. performed experiments and analyzed data; G.U. performed immunoblot analyses; J. Löttscher performed calcium-flux experiments; P.D. performed migration experiments; C.M.S. examined and scored the histopathological samples; J.D.W. performed immunoblot, RT-PCR, migration, and calcium-flux experiments; G.P. and G.R.B. established glutaminase-activity assays; A.-K.W., J.G., and N.K. performed MSSA tissue cage experiments; A.E. and L.B. provided clinical samples for acetate measurements; K.R. measured calcium and phosphate concentrations; J. Löliger and N.A. helped with metabolic tracing experiments; O.P.S. and S.H. performed PCR arrays; and C.H. designed, supervised, and coordinated the study and wrote the manuscript. All authors revised the manuscript and approved its final version.

### DECLARATION OF INTERESTS

The authors declare no conflicts of interest.

Received: August 17, 2019

Revised: April 21, 2020

Accepted: July 12, 2020

Published: July 31, 2020

### Figure 4. Acetate Suppresses Immunopathology at Sites of Infection and Modulates Tissue Remodeling

(A) LmOVA-immunized mice were i.p. re-infected with 10<sup>5</sup> CFU LmOVA in the presence (blue) or absence (black) of 10 mM acetate, and bacterial burdens in spleen and liver were assessed by bacterial plating 24 h post-infection.  
(B) LDH levels in the peritoneal fluid of mice described in (A) were analyzed using a commercially available assay kit.  
(C) IFN- $\gamma$  levels in the peritoneal fluid of mice described in (A) were determined by cytometric bead array.  
(D) Peritoneal morphology on formalin-fixed, paraffin-embedded samples stained with elastica van Gieson. Shown are representative samples of one control (Ctr) and one acetate-treated (Ac) animal. Peritoneal thickness was quantified (right panel).  
(E) Volcano plot of PCR array analysis of the peritoneal samples shown in (D). Red-highlighted genes were upregulated; green-highlighted genes downregulated in the presence of acetate.  
(F) Schematic depiction of the proposed model of acetate, playing opposing roles during an immune response in a time- and context-dependent manner. Each dot in (A)–(D) represents one mouse. Shown are pooled data from 2 independent experiments with 3–7 animals per group. Lines indicate means; error bars are SD. Dashed lines in (A) and (C) indicate the detection limit. t test was used to compare the groups. \*p < 0.05, \*\*p < 0.01.

REFERENCES

- Balmer, M.L., Ma, E.H., Bantug, G.R., Grählert, J., Pfister, S., Glatter, T., Jauch, A., Dimeloe, S., Slack, E., Dehio, P., et al. (2016). Memory CD8(+) T cells require increased concentrations of acetate induced by stress for optimal function. *Immunity* *44*, 1312–1324.
- Beisel, W.R. (1975). Metabolic response to infection. *Annu. Rev. Med.* *26*, 9–20.
- Blagih, J., Coulombe, F., Vincent, E.E., Dupuy, F., Galicia-Vázquez, G., Yurchenko, E., Raisi, T.C., van der Windt, G.J.W., Viollet, B., Pearce, E.L., et al. (2015). The energy sensor AMPK regulates T cell metabolic adaptation and effector responses in vivo. *Immunity* *42*, 41–54.
- Brown, G., Singer, A., Proudfoot, M., Skarina, T., Kim, Y., Chang, C., Dementieva, I., Kuznetsova, E., Gonzalez, C.F., Joachimiak, A., et al. (2008). Functional and structural characterization of four glutaminases from *Escherichia coli* and *Bacillus subtilis*. *Biochemistry* *47*, 5724–5735.
- Comerford, S.A., Huang, Z., Du, X., Wang, Y., Cai, L., Witkiewicz, A.K., Walters, H., Tantawy, M.N., Fu, A., Manning, H.C., et al. (2014). Acetate dependence of cancer cells via HIF-1 $\alpha$ . *Cell* *159*, 1591–1602.
- Dong, F., Wang, B., Zhang, L., Tang, H., Li, J., and Wang, Y. (2012). Metabolic response to *Klebsiella pneumoniae* infection in an experimental rat model. *PLoS ONE* *7*, e51060.
- Faubert, B., Vincent, E.E., Griss, T., Samborska, B., Izreig, S., Svensson, R.U., Mamer, O.A., Avizonis, D., Shackelford, D.B., Shaw, R.J., and Jones, R.G. (2014). Loss of the tumor suppressor LKB1 promotes metabolic reprogramming of cancer cells via HIF-1 $\alpha$ . *Proc. Natl. Acad. Sci. USA* *111*, 2554–2559.
- Ferreira, A.P.S., Cassago, A., Gonçalves, K. de A., Dias, M.M., Adamoski, D., Ascenção, C.F.R., Honorato, R.V., de Oliveira, J.F., Ferreira, I.M., Fomezari, C., et al. (2013). Active glutaminase C self-assembles into a supratetrameric oligomer that can be disrupted by an allosteric inhibitor. *J. Biol. Chem.* *288*, 28009–28020.
- Harty, J.T., and Badovinac, V.P. (2008). Shaping and reshaping CD8+ T-cell memory. *Nat. Rev. Immunol.* *8*, 107–119.
- Hoverstad, T., and Midtvedt, T. (1986). Short-chain fatty acids in germfree mice and rats. *J. Nutr.* *116*, 1772–1776.
- Huda-Faujan, N., Abdulamir, A.S., Fatimah, A.B., Anas, O.M., Shuhaimi, M., Yazid, A.M., and Loong, Y.Y. (2010). The impact of the level of the intestinal short chain Fatty acids in inflammatory bowel disease patients versus healthy subjects. *Open Biochem. J.* *4*, 53–58.
- Iwata, M., Hirakiyama, A., Eshima, Y., Kagechika, H., Kato, C., and Song, S.-Y. (2004). Retinoic acid imprints gut-homing specificity on T cells. *Immunity* *21*, 527–538.
- John, A.-K., Schmalzer, M., Khanna, N., and Landmann, R. (2011). Reversible daptomycin tolerance of adherent staphylococci in an implant infection model. *Antimicrob. Agents Chemother.* *55*, 3510–3516.
- Kunkel, E.J., and Butcher, E.C. (2002). Chemokines and the tissue-specific migration of lymphocytes. *Immunity* *16*, 1–4.
- Li, Y., Erickson, J.W., Stalnecker, C.A., Katt, W.P., Huang, Q., Cerione, R.A., and Ramachandran, S. (2016). Mechanistic basis of glutaminase activation: a key enzyme that promotes glutamine metabolism in cancer cells. *J. Biol. Chem.* *291*, 20900–20910.
- McGuirk, S., Gravel, S.-P., Deblis, G., Papadopolis, D.J., Faubert, B., Wegner, A., Hiller, K., Avizonis, D., Akavia, U.D., Jones, R.G., et al. (2013). PGC-1 $\alpha$  supports glutamine metabolism in breast cancer. *Cancer Metab.* *1*, 22.
- Mizuno, M., Ito, Y., Hepburn, N., Mizuno, T., Noda, Y., Yuzawa, Y., Harris, C.L., Morgan, B.P., and Matsuo, S. (2009). Zymosan, but not lipopolysaccharide, triggers severe and progressive peritoneal injury accompanied by complement activation in a rat peritonitis model. *J. Immunol.* *183*, 1403–1412.
- Nguyen, C.T.Q., Shetty, V., and Maresso, A.W. (2015). Global metabolomic analysis of a mammalian host infected with *Bacillus anthracis*. *Infect. Immun.* *83*, 4811–4825.
- Nowakowska, J., Landmann, R., and Khanna, N. (2014). Foreign body infection models to study host-pathogen response and antimicrobial tolerance of bacterial biofilm. *Antibiotics (Basel)* *3*, 378–397.
- O'Donovan, D.J., and Lotspeich, W.D. (1966). Activation of kidney mitochondrial glutaminase by inorganic phosphate and organic acids. *Nature* *212*, 930–932.
- Pappu, R., Schwab, S.R., Cornelissen, I., Pereira, J.P., Regard, J.B., Xu, Y., Camerer, E., Zheng, Y.-W., Huang, Y., Cyster, J.G., and Coughlin, S.R. (2007). Promotion of lymphocyte egress into blood and lymph by distinct sources of sphingosine-1-phosphate. *Science* *316*, 295–298.
- Reiss, Y., Proudfoot, A.E., Power, C.A., Campbell, J.J., and Butcher, E.C. (2001). CC chemokine receptor (CCR)4 and the CCR10 ligand cutaneous T cell-attracting chemokine (CTACK) in lymphocyte trafficking to inflamed skin. *J. Exp. Med.* *194*, 1541–1547.
- Rouse, B.T., and Sehrawat, S. (2010). Immunity and immunopathology to viruses: what decides the outcome? *Nat. Rev. Immunol.* *10*, 514–526.
- Sigmundsdottir, H., and Butcher, E.C. (2008). Environmental cues, dendritic cells and the programming of tissue-selective lymphocyte trafficking. *Nat. Immunol.* *9*, 981–987.
- Stalnecker, C.A., Erickson, J.W., and Cerione, R.A. (2017). Conformational changes in the activation loop of mitochondrial glutaminase C: A direct fluorescence readout that distinguishes the binding of allosteric inhibitors from activators. *J. Biol. Chem.* *292*, 6095–6107.
- Svensson, M., Johansson-Lindbom, B., Zapata, F., Jaensson, E., Austenaa, L.M., Blomhoff, R., and Agace, W.W. (2008). Retinoic acid receptor signaling levels and antigen dose regulate gut homing receptor expression on CD8+ T cells. *Mucosal Immunol.* *1*, 38–48.
- Tremaroli, V., and Bäckhed, F. (2012). Functional interactions between the gut microbiota and host metabolism. *Nature* *489*, 242–249.
- Trompette, A., Gollwitzer, E.S., Pattaroni, C., Lopez-Mejia, I.C., Riva, E., Pernet, J., Ubags, N., Fajas, L., Nicod, L.P., and Marsland, B.J. (2018). Dietary fiber confers protection against flu by shaping Ly6c<sup>+</sup> patrolling monocyte hematopoiesis and CD8<sup>+</sup> T cell metabolism. *Immunity* *48*, 992–1005.e8.
- van der Windt, G.J.W., Everts, B., Chang, C.-H., Curtis, J.D., Freitas, T.C., Amiel, E., Pearce, E.J., and Pearce, E.L. (2012). Mitochondrial respiratory capacity is a critical regulator of CD8+ T cell memory development. *Immunity* *36*, 68–78.
- van der Windt, G.J.W., O'Sullivan, D., Everts, B., Huang, S.C.-C., Buck, M.D., Curtis, J.D., Chang, C.-H., Smith, A.M., Ai, T., Faubert, B., et al. (2013). CD8 memory T cells have a bioenergetic advantage that underlies their rapid recall ability. *Proc. Natl. Acad. Sci. USA* *110*, 14336–14341.

Q6 Q7 STAR★METHODS

KEY RESOURCES TABLE

REAGENT or RESOURCE	SOURCE	IDENTIFIER
<b>Antibodies</b>		
BUV395 rat anti-mouse CD44	BD	Cat# 740215
APC rat anti-mouse CD8	Biolegend	Cat# 100712
BV421 hamster anti-mouse KLRG1	Biolegend	Cat# 138413
PE rat anti-mouse CD62L	Biolegend	Cat# 104408
APC-Cy7 rat anti-mouse CD43	Biolegend	Cat# 121220
BV421 rat anti-mouse PDL1	Biolegend	Cat# 124315
PE-Cy5 rat anti-mouse CD127	eBioscience	Cat# 15-1271-82
PE rat anti-mouse CD25	Biolegend	Cat# 101904
BV510 hamster anti-mouse CD27	Biolegend	Cat# 124229
FITC rat anti-mouse CD3	BD	Cat# 555274
PE rat anti-mouse CD8	Biolegend	Cat# 100708
APC mouse anti-human CD62L	ImmunoTools	Cat# 21819626
Pacific Blue anti-CD45RA	Beckman Coulter	Cat# A86050
<b>Bacterial and Virus Strains</b>		
Listeria monocytogenes expressing chicken Ovalbumin (AA134–387)	Prof. Ed Palmer, University Basel, CH	N/A
<b>Biological Samples</b>		
Human body fluids	University Hospital Basel	N/A
<b>Chemicals, Peptides, and Recombinant Proteins</b>		
Liberase TL Research Grade	Roche	Cat#05 401 020 001
APC Annexin V	Immunotools	Cat#31490016
BPTES	Sigma Aldrich	Cat#SML0601
SB204990	Tocris	Cat#4962
Recombinant murine CXCL12	Peprotech	Cat#250-20A
Recombinant human glutaminase	R&D Systems	Cat#10115-GL-020
Glutaminase from <i>E. coli</i>	Megazyme	Cat#E-GLUTEC
<b>Critical Commercial Assays</b>		
Acetate fluorimetric assay kit	BioAssay Systems	Cat#EOAC-100
LDH Assay Kit	Abcam	Cat#ab102526
Glutaminase Microplate Assay Kit	Cohesion Biosciences	Cat#CAK1065
<b>Experimental Models: Organisms/Strains</b>		
Mouse: B6.129S6-Rag2tm1Fwa Tg(TcraTcrb)1100Mjb	Taconic	Model #2334
Mouse: C57BL/6	Charles River and Janvier	N/A
<b>Oligonucleotides</b>		
ms ACSS1 (forward 5'-GTTTGGGACA CTCCTTACCATAC-3' and reverse 5'-AGGCAGTTGACAGACACATTC-3')	Invitrogen	This paper
ms ACSS2 (forward 5'-GTGAAAGGAT CTTGGATTCCAGT-3' and reverse 5'-CAGATGTTTGACCACAATGCAG-3')	Invitrogen	This paper
GIs: Mm01257297_m1	Thermo Fisher	Cat#4331182
lfn9: Mm01168134_m1	Thermo Fisher	Cat#4331182

(Continued on next page)

**Continued**

REAGENT or RESOURCE	SOURCE	IDENTIFIER
ms 18S primers (forward 5'-GGGAGC CTGAGAAACGGC-3' and reverse 5'-GGGTCGGGAGTGGGTAATTT-3')	Microsynth	This paper
hs ACSS1 (forward 5'-CACAGGACAG ACAACAAGGTC-3' and reverse 5'-CCTGGGTATGGAACGATGCC-3')	Invitrogen	This paper
hs ACSS2 (forward 5'-AAAGGAGCAA CTACCAACATCTG-3' and reverse 5'-GCTGAACTGACACACTTGGAC-3')	Invitrogen	This paper
Human 18S	Applied Biosystems	Cat#4310893E
Recombinant DNA		
pGEX-4T-1-GLS2_WT (C-terminal GST)	Genscript	N/A
pGEX-4T-1-GLS2_K253A (C-terminal GST)	Genscript	N/A
Software and Algorithms		
FlowJo	BD	<a href="https://www.flowjo.com">https://www.flowjo.com</a>
GOLD Suite v5.7.0	The Cambridge Crystallographic Data Centre, Cambridge, UK	<a href="https://www.ch.cam.ac.uk/computing/software/gold-suite">https://www.ch.cam.ac.uk/computing/software/gold-suite</a>
PyMol v1.3	Schrödinger	<a href="https://pymol.org/2/">https://pymol.org/2/</a>
ImageJ	N/A	<a href="https://imagej.net/Welcome">https://imagej.net/Welcome</a>
GraphPad Prism	N/A	<a href="https://www.graphpad.com/scientific-software/prism/">https://www.graphpad.com/scientific-software/prism/</a>

**RESOURCE AVAILABILITY**

**Lead Contact**

Further information and requests for resources and reagents should be directed to and will be fulfilled by the Lead Contact, Christoph Hess ([ch818@cam.ac.uk](mailto:ch818@cam.ac.uk); [chess@uhbs.ch](mailto:chess@uhbs.ch)).

**Materials Availability**

This study did not generate new unique reagents.

**Data and Code Availability**

The published article includes all datasets generated or analyzed during this study.

**EXPERIMENTAL MODEL AND SUBJECT DETAILS**

**Animal Husbandry**

Male and female C57BL/6 or MHC class I-restricted OVA-specific T cell receptor (OT-I) transgenic mice were 6-8 weeks of age and housed in IVC cages on racks in a room with controlled temperature (22–24°C) and humidity (40%–60%). Mice were maintained on a 12 h light-dark cycle. All mice were fed a standard diet (Kliba AG, #3436 EX). Health checks were conducted on all mice at least once daily. For experimental control groups, littermates were used. All animal experiments were approved by the Animal Care Committee of the Veterinary Office Basel, Switzerland.

**Human Abscess Fluids**

Human abscess fluids were obtained from the division of Clinical Microbiology of the University Hospital Basel after informed consent of the patients and ethical approval of the ethics committee of both Basels. As controls, non-inflamed samples (e.g., sterile ascites, cyst-fluids, pleural transudate) were used. Samples were stored at 4°C prior to measurement. Patient characteristics are summarized in [Table 1](#).

**Isolation of Human Effector Memory (EM) CD8<sup>+</sup> T Cells**

Peripheral blood mononuclear cells were isolated by standard density-gradient centrifugation protocols (Lymphoprep; Fresenius Kabi) from healthy male and female blood donors, > 18 years of age. Results were not stratified by age or sex, since we did not have this information at the time of analysis. MACS beads and LS columns (both Milteny Biotec) were used to sort CD8<sup>+</sup> positive T cells. The positively selected CD8<sup>+</sup> T cells were incubated with APC anti-CD62L mAb (ImmunoTools) and Pacific Blue anti-CD45RA

(Beckman Coulter) and sorted by flow cytometry (BD FACSAria III or BD Influx Cell Sorter). Experiments using blood donor derived cells were approved by the blood transfusion service of the Swiss Red Cross.

### Cell Culture

Primary cells of male and female mice were cultured in RPMI medium (RPMI 1640 containing 10% FCS, 100 U/mL penicillin, 100  $\mu$ g streptomycin, 0.29 mg/mL L-glutamine, 50  $\mu$ M 2-Mercaptoethanol) at 37°C and 5% CO<sub>2</sub>.

### METHOD DETAILS

#### *In Vitro* Memory Differentiation

Memory OT-I T cells were generated as described previously (Balmer et al., 2016; van der Windt et al., 2013). Briefly, the lymph nodes from MHC class I-restricted OVA-specific T cell receptor (OT-I) transgenic mice and the spleen of C57BL/6 mice were aseptically removed and incubated in liberase TL (Roche) for 30 min. After mashing through a 70  $\mu$ m cell strainer (BD Biosciences), red blood cells were lysed with RBC Lysis Buffer Solution (eBioscience). The isolated cell suspensions were washed in RPMI medium (RPMI 1640 containing 10% FCS, 100 U/mL penicillin, 100  $\mu$ g streptomycin, 0.29 mg/mL L-glutamine, 50  $\mu$ M 2-Mercaptoethanol (Life Technologies)) and re-suspended to 10<sup>6</sup> cells/mL. The splenocytes and OT-I cells were pooled in a ratio of 1:1 and activated with OVA peptide (Eurogentec) at 10<sup>-9</sup> M at 37°C for 3 days. The cells were then washed and re-suspended to 2  $\times$  10<sup>6</sup> cells/mL and cultured in the presence of IL-15 (10 ng/mL) at 37°C for another 3 days to generate OVA-specific memory CD8<sup>+</sup> T cells. Phenotyping was performed using BUV395-anti CD44 (BD), APC-anti CD8, BV421-anti KLRG1, PE-anti-CD62L, APC-Cy7-anti CD43, BV421-anti PDL1, PE-anti-CD25, BV510-anti CD27 (all Biolegend) and PE-Cy5-anti CD127 (eBioscience).

#### Acetate Measurement in Murine and Human Samples

Acetate concentrations in peritoneal fluids and human samples were determined using the acetate fluorimetric assay kit (Bioassay Systems), following the manufacturer's instructions.

#### Measurement of Cell Viability

To measure the viability, 10<sup>5</sup> mouse or human memory CD8<sup>+</sup> T cells were plated in a 96-well plate in RPMI medium. The cells were incubated at 37°C for up to 7 days. The cells were washed in Annexin V Binding Buffer (BD Pharmingen) and stained with APC Annexin V (ImmunoTools) and PI (Sigma Aldrich). Samples were acquired on an Accuri® C6 Flow Cytometer and analyzed with FlowJo-Software (FlowJo 10.2). Viable cells were defined as Annexin V and PI double negative. Where indicated, cells were incubated in presence of BPTES (Sigma Aldrich) at 50  $\mu$ M or in glutamine-free RPMI containing dialyzed FCS (Life Technologies).

#### Transwell migration assay

For the *in vitro* migration assay 2-5  $\times$  10<sup>5</sup> cells were resuspended in 80% full medium and 20% PBS, supplemented with varying concentration of sodium acetate, calcium chloride and sodium chloride. 100  $\mu$ L of cell suspension was seeded in 5  $\mu$ m pore cell culture inserts (Sigma, CLS3421) with 500  $\mu$ L of the corresponding medium in the well. After 3 h incubation at 37°C, the volumes in the insert and the well were measured with a pipette. The cell density was measured by acquiring 30  $\mu$ L of the insert and well with a CytoFlex flow cytometer (Beckman Coulter) by counting the number of events in the live gate using FlowJo. The translocation index was calculated by dividing the cell number of the cell culture insert with the total cell number. Every condition was assessed by technical triplicates and every experiment was repeated at least three times. Where indicated, CXCL12 (Peprotech) at 50 ng/mL was used.

#### Murine Peritonitis Model

C57BL/6 mice were intra-peritoneally (i.p.) infected with 5000 CFU *Listeria monocytogenes* expressing the OVA-peptide (LmOVA). 28 days later, mice were re-infected with 10<sup>5</sup> CFU LmOVA i.p. in presence or absence of 5 mM acetate. Mice were sacrificed 24 h later and peritoneal fluid, spleen, liver and serum harvested. Spleens and livers were homogenized in 0.5% Terigitol/PBS using a Tissue-lyser (QIAGEN) and sterile stainless-steel ball bearings. Organ suspensions were then plated on BHI agar-plates and colonies counted upon 24 h incubation at 37°C. Peritoneal fluids were centrifuged and the cells analyzed by flow-cytometry upon staining with FITC-anti-CD3, BUV395-anti CD44 (both BD), BV421-anti PDL1, APC-Cy7-anti CD43, BV510-anti CD27 and PE-anti CD8 antibodies, Zombie-Red viability staining (all Biolegend) or by RT-PCR upon MACS-purification and storage in Trizol Reagent (Thermo Fisher Scientific). Peritoneal fluids and sera were frozen at -80°C prior to further analysis. LDH concentrations in peritoneal fluids were measured using a commercially available assay kit (Abcam). All experiments were performed in accordance with local rules for the care and use of laboratory animals.

#### *S. aureus* Tissue Cage Model

The mouse model of foreign-body infection (John et al., 2011; Nowakowska et al., 2014) was used in the present study. Briefly, a sterile tissue cage (Angst + Pfister AG, Zurich, Switzerland) was implanted subcutaneously in the back of female C57BL/6 mice, 13 weeks old (janvierlab, France). After complete wound healing (2 weeks), cages were tested for sterility by culturing the aspirated tissue cage fluid (TCF). Teflon cages were infected with 785 CFU of MSSA ATCC 29213. The infection was confirmed at day 1 directly

before treatment start by plating. Mice were i.p. treated twice a day with 5% glucose for 11 days. Tissue cage fluid (TCF) was aspirated at different time points (day 3, 6, 9, 11 and 14) and appropriate dilutions were plated to determine the amount of planktonic MSSA. Tissue cage fluids were then analyzed for acetate, calcium and phosphate levels and CD8<sup>+</sup> T cells isolated by MACS-purification and frozen in Trizol Reagent (Thermo Fisher Scientific). For phenotyping, cells were stained with APC-anti CD8 (Biolegend), BUV395-anti CD44 (BD), PE-anti CD62L (Biolegend) antibodies and Zombie-Red Viability staining (Biolegend).

### Histology

Small pieces (0.5 × 0.5 cm) of peritoneum were fixed in 4% formaldehyde for 24 h. Samples were then paraffin-embedded, cut, and stained with H&E and elastica van Gieson on an automated-stainer according to standard procedures. Peritoneal thickness was measured from the mesothelial surface to the border of the loose connective tissue between compact zone and muscular layer by a board-certified pathologist in a blinded manner as described in (Mizuno et al., 2009).

### Seahorse Experiments

Oxygen consumption rates (OCR, in pMoles/min) and extracellular acidification rates (ECAR, in mpH/min) were measured in plated cells ( $2.5 \times 10^5$  per well) kept in serum-free unbuffered RPMI-1640 medium (Sigma-Aldrich), under basal conditions, and in response to OVA-peptide (10  $\mu$ M) or acetate (5 mM) injection using the instrument's multi-injection ports. Where indicated, cells were pre-treated with the ACLY-inhibitor SB204990 (Tocris) at 30  $\mu$ M or BPTES (Sigma Aldrich) at 50  $\mu$ M 2 h prior to and during metabolic flux analysis or vehicle control. All data were generated using the XF-96 Extracellular Flux Analyzer (Seahorse Bioscience).

### Metabolic Tracing

GC-MS metabolite analysis was conducted as previously described (Blagih et al., 2015) (Balmer et al., 2016). Briefly,  $5 \times 10^6$  IL-15 expanded OT-1 memory cells were cultured in standard or glutamine-free RPMI (with 10% dialyzed FCS) containing 10 mM 1,2-[13C]-acetate or 10 mM 13C-glutamine (Cambridge Isotope Laboratories) for 6 h. Metabolites were extracted from cells using ice-cold 80% methanol, followed by sonication and removal of cellular debris by centrifugation at 4°C. Metabolite extracts were dried, derivatized as tert-butylidimethylsilyl (TBDMS) esters, and analyzed via GC-MS as previously described (Faubert et al., 2014). Uniformly deuterated myristic acid (750 ng/sample) was added as an internal standard following cellular metabolite extraction, and metabolite abundance was expressed relative to the internal standard and normalized to cell number. Mass isotopomer distribution was determined using a custom algorithm developed at McGill University, CA (McGuirk et al., 2013).

### Quantitative PCR

Quantitative PCR for mouse ACSS1 and ACSS2 mRNA was done in triplicates with SYBR Green Supermix (Promega). The following primers were used: ms ACSS1 (forward 5'-GTTTGGGACACTCCTTACCATAC-3' and reverse 5'-AGGCAGTTGACAGACACATTC-3'), ms ACSS2 (forward 5'-GTGAAAGGATCTTGGATTCCAGT-3' and reverse 5'-CAGATGTTTGACCACAATGCAG-3') (both Invitrogen). The following primers were used to analyze glutaminase mRNA: Mm01257297\_m1 (Thermo Fisher Scientific). *IFN $\gamma$*  mRNA was measured using primers Mm01168134\_m1 (Thermo Fisher Scientific). As a housekeeping gene mouse 18S mRNA was measured using ms 18S primers (forward 5'-GGGAGCCTGAGAAACGGC-3' and reverse 5'-GGGTGCGGAGTGGGTAATTT-3') (Microsynth). Quantitative PCR for human ACSS1 and ACSS2 mRNA was done in triplicates with SYBR Green Supermix (Promega). The following primers were used: hs ACSS1 (forward 5'-CACAGGACAGACAACAAGGTC-3' and reverse 5'-CCTGGGTATGGAACGATGCC-3'), hs ACSS2 (forward 5'-AAAGGAGCAACTACCAACATCTG-3' and reverse 5'-GCTGAACTGACACACTTGGAC-3') (both Invitrogen). As a housekeeping gene 18S was used (4310893E, Applied Biosystems). Peritoneal immunopathology was assessed using the mouse Wound Healing RT<sup>2</sup> Profiler PCR Array following the manufacturer's instructions (QIAGEN). RNA-quality was checked prior to the assay using the Bioanalyzer RNA-kit (Agilent).

### Glutaminase Activity Assay

To analyze the activity of glutaminase in memory CD8<sup>+</sup> T cells, the Glutaminase Microplate Assay Kit (Cohesion Biosciences) was used. After incubation, cells (4 Mio) were sonicated in the assay buffer (40  $\mu$ l) provided with the kit and then processed according to the manufacturer's instructions. Recombinant human glutaminase at 1  $\mu$ g/mL (R&D Systems) and glutaminase from *E. coli* at 6 U/mL (Megazyme) were tested in the Glutaminase Microplate Assay (Cohesion Biosciences).

### Glutaminase-Acetate In Silico Docking

We used a template of the human glutaminase co-crystallized with bound glutamine (PDB ID 3VP0). The three-dimensional structure of acetate was constructed *ab initio* in Chem3D Pro v14.0 (CambridgeSoft, Cambridge, UK) and energy-minimized using the integrated MM2 force field. The binding site of acetate was defined as being within 20 Å of the centroid around the  $\alpha$ -carbon of Y446, a centrally located residue that interacts with glutamine in the substrate binding site. Acetate was docked as a flexible ligand into the ligand-occupied structure using GOLD Suite v5.7.0 (The Cambridge Crystallographic Data Centre, Cambridge, UK) with the GoldScore function and default settings. Ten docked poses were generated and visualized with PyMol v1.3.

### Glutaminase Mutagenesis

Human GLS2 was cloned into the multiple cloning site of a pGEX-4T-1 bacterial expression vector containing a C-terminal glutathione-S-transferase (GST) tag. The K253A variant was generated by site-directed mutagenesis which corresponds to the GLS1 sequence K→A shown in [Figure 2L](#). The *E. coli* strain BL21(DE3) was then transformed with wild type or K253A mutant pGEX-4T-1-GLS2 vectors. Recombinant GLS2-GST was purified from bacterial cell lysate using GST hiTRAP and Superdex 200 columns and eluted in 5mM Tris, 150mM HCl buffer (pH 7.5). Wildtype and mutant glutaminase was used at a concentration of 1 μg/mL for measuring glutaminase activity as described above.

### Calcium Flux

*In vitro* differentiated memory OT-I T cells were loaded with 1 μM Fluo4 (Invitrogen) and 1 μM Fura Red (Invitrogen) with indicated acetate or calcium concentrations for 30 min at 37°C. After washing, T cells were activated with 10 μM OVA-peptide under continuous acquisition using an Accuri C6 (BD) or Cytotflex (Beckmann coulter) flow cytometer. Analysis was performed with FlowJo software using kinetics tool (ratio of geometric mean fluorescence intensity of Fluo4/FuraRed) and Prism software.

### Calcium and Phosphate Quantification

Calcium and phosphate concentrations were measured in collaboration with the diagnostics department of the University Hospital Basel using a photometric Assay (Cobas, Roche). For *in vitro* calcium-measurements, PBS was supplemented with increasing concentrations of acetate and calcium-concentrations measured immediately.

### Intracellular Cytokine Staining

200,000 cells per condition were re-activated with CD3/CD28 beads (1:10) or OVA-peptide (10 μM) in presence or absence of the indicated concentrations of acetate or calcium for 4 h. Brefeldin A (Biolegend) was added after 1 h of incubation. Fixation and permeabilization with BD Cytofix/Cytoperm and BD Perm/Wash was done according to the instruction of the manufacturer (BD Biosciences). Cells were then stained with FITC-anti-human IFN-γ (BD Biosciences) or FITC-anti-mouse IFN-γ (Biolegend), acquired on an Accuri C6 Flow Cytometer and analyzed using FlowJo-Software (FlowJo 10.2).

### Cytometric Bead Array

Cytokine concentrations in cell culture supernatants and peritoneal fluids were determined using the LegendPlex cytometric bead Array Th1-Pannel (Biolegend), according to the manufacturer's instructions.

### Immunoblot Analysis

Memory T cells were lysed in RIPA buffer (Thermo Scientific) containing protease- and phosphatase-inhibitors (Roche, #05 892 970 001 and #04 906 837 001), and protein concentrations determined with a BCA protein assay kit (Thermo Scientific). Whole-cell lysates were separated by 4%–20% SDS-PAGE and transferred to nitrocellulose or PVDF membranes. Membranes were probed with anti-glutaminase mAb (Protein Tech, #19958-1-AP) and anti-actin mAb (Sigma #A1978). Blots were then stained with the appropriate secondary antibody (IRDye 800CW- conjugated goat polyclonal antibody to rabbit IgG (926-32211) from LI-COR). The Odyssey imaging system (LICOR) was used for detection, and the ImageJ software (1.48v) for quantification.

## QUANTIFICATION AND STATISTICAL ANALYSIS

Differences were analyzed for statistical significance using Prism 7 for Macintosh (GraphPad Software Inc.). The details of the tests carried out are indicated in each figure legend. Where data were approximately normally distributed, values were compared using either a Student's t test, one-way or two-way ANOVA. Where data were non-normally distributed Wilcoxon-tests were applied. In all cases, p values < 0.05 were considered significant.